Proceedings of the 2024
31th International Conference on Nuclear Engineering
ICONE31
August 4-8, 2024, Prague, Czech Republic

ICONE31-133230

FLUID-STRUCTURE-SOIL INTERACTION STUDY FOR NUCLEAR FACILITIES WITH LARGE POOL WATER CONSIDERING NONLINEAR STRUCTURAL BEHAVIOR

Yuki Sato
JGC Corporation
Kanagawa, Japan

Dan M. Ghiocel
Ghiocel Predictive Technologies, Inc.
New York, USA

Shunji Kataoka
JGC Corporation
Kanagawa, Japan

Yasutomi Morimoto
JGC Corporation
Kanagawa, Japan

ABSTRACT

This study investigates the effects of the Fluid-Structure-Soil Interaction (FSSI) on the seismic responses of a deeply embedded nuclear facility with large water pools under severe earthquakes. This paper presents new seismic analysis method considering FSSI using 3D FEM for deeply embedded typical RC (Reinforced Concrete) shear wall nuclear buildings. In the new method, the commercial SSI analysis software, ACS SASSI was used with Option AA-F, which treats ANSYS fluid element FLUID80 dynamic matrices in ACS SASSI environment. By using the method it was confirmed that large pool water in the building provides significant local deformation of the pool walls, while the effects on other part of the structures are almost negligible from engineering point of view. To investigate more with the structure behavior during severe earthquakes, the nonlinear behavior of the structure was also taken into account with the new FSSI method using ACS SASSI NQA Option NON. To model the RC wall nonlinear behavior, their nonlinear backbone curves (BBCs) were computed using both Japanese and America standards. Then, the nonlinear analysis responses with both standards were compared. It was confirmed that the nonlinear structure behavior produced a visible shift of the ISRS spectral peak responses to the lower frequencies in comparison with the response of linear analysis. Also, although some significant differences of seismic responses were not observed between Japanese standard and American standard, it was confirmed that the differences of formulae in each code were reflected on their seismic responses.

Keywords: soil-structure interaction, fluid-structure interaction, nonlinear analysis, RC structure, 3D FEM

NOMENCLATURE

$\propto$	Coefficient defining the relative contribution of concrete strength to nominal wall shear strength (unitless)
E_C	Young's modulus of concrete (N/mm^2)
F_C	Compressive strength of concrete (N/mm^2)
f_c'	Specified compressive strength of concrete at cracking point (N/mm^2)
$f_t = 0.38\sqrt{F_C}$	Flexural tensile strength of concrete (N/mm^2)
f_y	Strength of concrete at yielding point (N/mm^2)
ϕ_1	Curvature of tensile steel bar at cracking point (1/mm)
ϕ_2	Curvature of tensile steel bar at yielding point (1/mm)
ϕ_3	Curvature of tensile steel bar at ultimate point (1/mm)
G	Shear modulus of elasticity of concrete (N/mm^2)
γ_1	Shear strain at cracking point (unitless)
γ_2	Shear strain at yielding point (unitless)
γ_3	Shear strain at ultimate point (unitless)
$M/(QD)$	Shear span ratio (unitless)
I_e	Effective section moment of inertia including rebars (mm^4)
M_1	Moment of tensile steel bar at cracking point (N*mm)
M_2	Moment of tensile steel bar at yielding point (N*mm)
M_3	Moment of tensile steel bar at ultimate point (N*mm)
P_H	Horizontal reinforcement ratio (unitless)
P_V	Vertical reinforcement ratio (unitless)
s_r	User defined reduction factor based on test data (unitless)
σ_v	Vertical axial compressive stress (positive for compression, N/mm^2)
τ_1	Shear stress at cracking point (N/mm^2)
τ_2	Shear stress at yielding point (N/mm^2)
τ_3	Shear stress at ultimate point (N/mm^2)
X_{nu}	Distance from compression edge to neutral axis at full plastic moment (mm)
Z_e	Effective section modulus including rebars (mm^3)

1. INTRODUCTION

Recently, comparing with precedent plant designs, more severe seismic input tends to be required for nuclear power plants (NPPs). The importance of seismic analysis methodology for nuclear facilities with large water reservoir has been increasing because the water mass affects the deformation of structures largely due to severe earthquakes. In the seismic modeling method in nuclear industry, modeling of fluid as well as modeling of structural nonlinearity have been considered as key factors for many years.

Regarding the fluid modeling methods coupling with SSI (Soil-Structural Interaction) analysis, some advanced modeling methods have been developed. As for modeling of structural nonlinearity, various methods of modeling have been proposed for the purpose of practical NPP designs. Recently, the SSI analysis modeling method with combination of fluid model and nonlinear structural model has been performed. The nonlinear structural behavior differs depending on back-bone curves (BBCs) and hysteretic models. This paper investigates how differences in the Japanese code and the American code affect the nonlinear behaviors of building structures with massive pools.

2. MATERIALS AND METHODS

2.1 Structure model and Site Conditions

As a sample of nuclear related buildings, an SSI model with and without large-size water pool inside of the building (hereinafter called "BLDG15 model) is used for this study. The overview of BLDG15 is shown in Figure 1. The water pool is located at the upper floor level.

The seismic input at ground surface in the horizontal and vertical directions is shown as Design Response Spectra (DRS) in Figure 2. This DRS is almost the same as NuScale SMR CSDRS [1]. The peak ground acceleration is set to 0.50 g for horizontal motions, and 0.40 g for the vertical motion, respectively. The site soil profile is described by a uniform deep soil deposit with an Vs of 800 m/s, Vp of 1,600 m/s, unit weight of 20 kN/m^3 with a S and P wave damping of 2%. These soil properties were considered as the iterated soil properties for the study.

To define the seismic motion input for the SSI analysis of the deeply embedded BLDG15 structure, the in-column Foundation Input Response Spectra (FIRS), which is to be set at the foundation level, need to be obtained for X, Y and Z directions. The in-column FIRS were calculated by the site response analysis using ACS SASSI SOIL module with the outcrop motion defined at foundation level as the user input, and the in-column motion at foundation level as the user output. The calculated in-column FIRS were shown in Figure 2. The SOIL module uses SHAKE methodology for computing the in-column soil motions at different depths.

In this study, for performing BLDG15 nonlinear structure SSI analysis, the maximum ground acceleration was increased by 60% to consider beyond design basis earthquake (BDBE) level with 0.80 g for horizontal acceleration and 0.64 g for vertical acceleration.

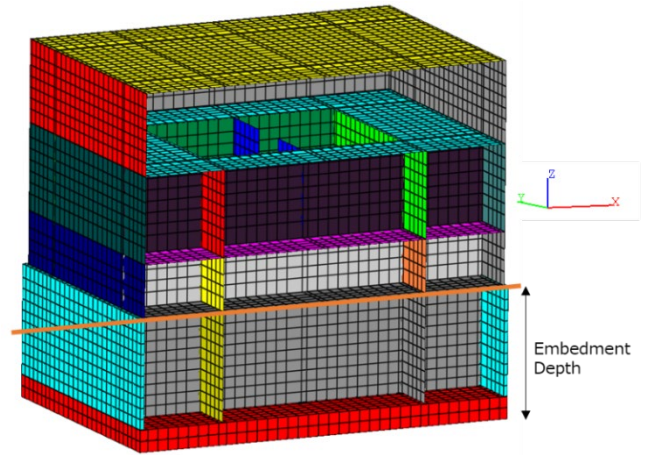

(A) WITHOUT-FLUID CASE

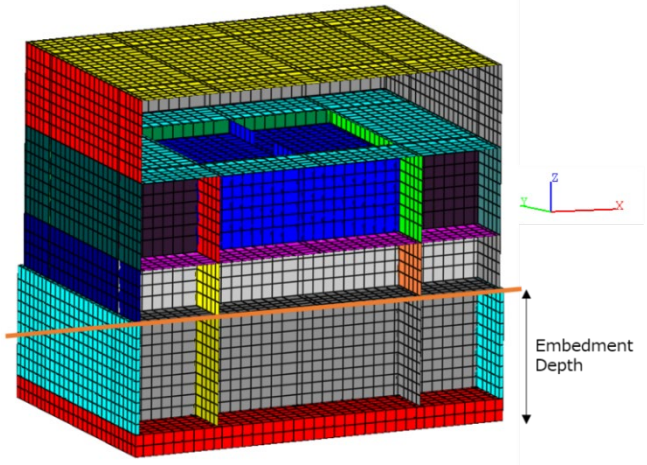

(B) WITH-FLUID CASE

FIGURE 1: BLDG15 MODEL

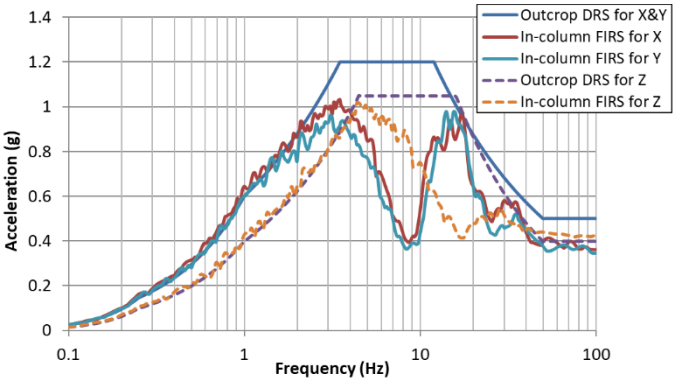

FIGURE 2: SEISMIC INPUT

2.2 Fast SSI Analysis of Deeply Embedded Structures

The ACS SASSI Flexible Volume Reduced-Order Modeling (FVROM) approach is a "theoretically exact" approach implemented in the ACS SASSI NQA software based on the condensation of the excavated soil impedance matrix at the foundation-soil interface nodes [2].

The FVROM SSI approach uses the condensation of the excavated soil impedance matrix $\mathbf{Z}(\omega)$ at the foundation-soil interface nodes (the other excavation internal nodes and ground surface nodes are eliminated). The excavated soil matrix $\mathbf{Z}(\omega)$ is computed based on the soil layering impedance matrix and the excavated soil dynamic matrix, i.e. $\mathbf{Z}(\omega) = \mathbf{X}(\omega) - \mathbf{C}^{e}(\omega)$ at each SSI frequency. The SSI system response is obtained using FVROM using the reduced-size excavated soil impedance matrix $\tilde{\mathbf{Z}}_{ii}(\omega)$ and the associated reduced-size load vector $\{\tilde{\mathbf{F}}_{i}(\omega)\}$ at each SSI frequency. The SSI system equation becomes for the reduced-size SSI system:

$$\begin{aligned} \left([\mathbf{C}^{s}_{ii}] + \tilde{\mathbf{Z}}_{ii}\right)\{\mathbf{U}_{i}\} + [\,\mathbf{C}^{s}_{is}]\{\mathbf{U}_{s}\} &= \{\tilde{\mathbf{F}}_{i}\} \\ [\mathbf{C}^{s}_{si}\,]\{\mathbf{U}_{i}\} + [\,\mathbf{C}^{s}_{ss}]\{\mathbf{U}_{s}\} &= \{\mathbf{0}\} \end{aligned} \qquad (1)$$

where $[\mathbf{C}^{s}]$ and $\{\mathbf{U}_{s}\}$ are the structure dynamic stiffness and the complex displacement solution. Indices s and i correspond to structure and soil interface degrees of freedom, respectively.

Since the excavated soil impedance variation in frequency is much smoother than the SSI response variation by the interpolation, it is highly efficient for speeding up the overall computational effort of SSI analysis. Only a reduced number of frequencies can be used for accurately computing the condensed soil impedance matrix and seismic load vector, and then, interpolating them for the rest of all other SSI frequencies. FVROM matrix condensation can be further combined with the efficient interpolation of the reduced-size soil impedance matrix in complex frequency. For practical applications, for the FVROM-INT approach a reduced number of condensation frequencies of 15-25 are usually sufficient for an accurate interpolation of the soil impedance interpolation. After the SSI response is computed, say for 200-250 SSI frequencies, this response is further interpolated for all Fourier frequencies used for describing the input motion data in the frequency domain. For more information, please see the paper [3].

2.3 Fluid Modeling for Seismic FSSI Analysis

The ACS SASSI Option AA-F is used to include the pool fluid substructure in the building model. The fluid elements, which are the ANSYS FLUID80 elements, are extracted by specific automatic procedure. Using ACS SASSI UI ANSYS model converter, two FE models topologically identical to the ANSYS model including structure and fluid were generated for ACS SASSI. The ANSYS 8-node FLUID80 elements were converted to 8-node ACS SASSI SOLIDF elements. These SOLIDF are "fake" SOLID elements, used as place holders for the FLUID80 substructure matrices inclusion, being used only for a model topology and equation mapping between the ANSYS and the ACS SASSI models.

The application of Option AA-F includes two stages:

Stage 1: *PREPARE ANSYS and ACS SASSI FSSI MODELS*:

Prepare the ANSYS FSSI FE model including a single or multiple FLUID80 element substructures (such as pools or vessels), and then, convert this model into an ACS SASSI model with "fake" SOLIDF. Then, delete all the non-fluid elements to retain only the FLUID80 substructures for which the dynamic property matrices can be extracted and assembled with ACS SASSI model matrices using a specialized ANSYS macro.

Stage 2: *RUN ACS SASSI FSSI ANALYSIS:*

Run FSSI analysis using the ACS SASSI FSSI model with the FILE80 substructure matrices integrated within the FSSI system matrices.

The fluid modeling for seismic FSSI analysis in ACS SASSI has been verified by conducting the comparison with other methods. The comparison confirmed that ACS SASSI FSSI model provides comparable results with other practical method [3].

2.4 Nonlinear RC Structure Modeling

Figure 3 describes the concept of the iterative hybrid frequency-time SSI approach as implemented in ACS SASSI Option NON. The iterative hybrid approach includes at each iteration two coupled analysis steps:

Step1: Perform an *equivalent-linear SSI analysis* in complex frequency via the SASSI approach to compute the structural displacements for each nonlinear RC wall, and then,

Step 2: Perform *a nonlinear time-domain hysteretic analysis* for each RC wall loaded with the SSI displacements from Step 1, to compute the in-plane shear and bending nonlinear wall responses using the standard-based back-bone curve (BBC) equations and the appropriate hysteretic models from the available software library.

The *equivalent-linear stiffness and damping for each RC wall* are computed based on the time domain nonlinear responses using either a constant or a variable maximum displacement reduction factor (DRF) applied at each SSI iteration. It should be noted that *Step 1* uses the *original, refined FE SSI model* (left plot in Figure 3) while *Step 2* uses a *reduced-order structural model* (right plot in Figure 3) using macro-mechanics models for simulating the RC wall hysteretic behavior. For more information, please see the paper [4].

Based on BLDG15 layout, the RC walls consisting of the buildings were divided into 8 sub-models. The selected RC walls modeled in sub-models are shown in Figure 4. The exterior RC wall sub-models, and the interior RC wall sub-models are shown in Figure 5 and 6, respectively.

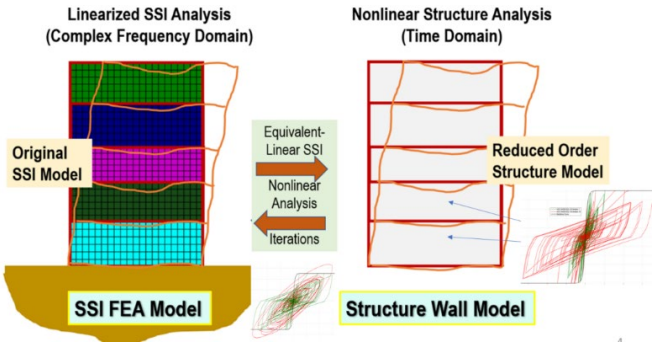

FIGURE 3: ITERATIVE HYBRID SSI APPROACH IMPLEMENTED IN ACS SASSI OPTION NON

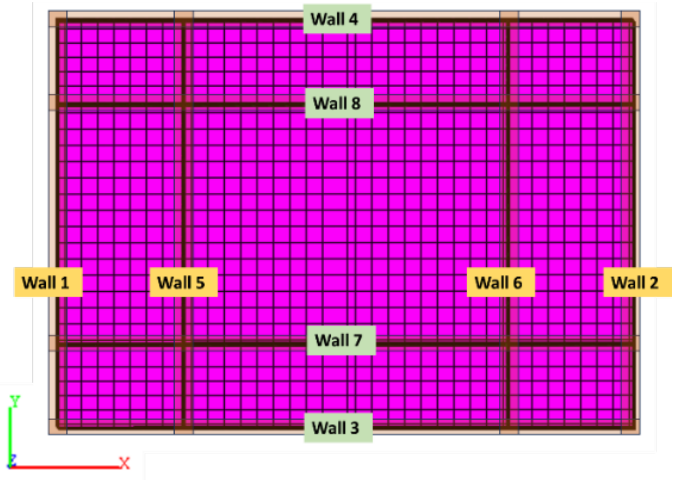

FIGURE 4: SELECTION OF BLDG15 NONLINEAR RC WALL SUB-MODELS

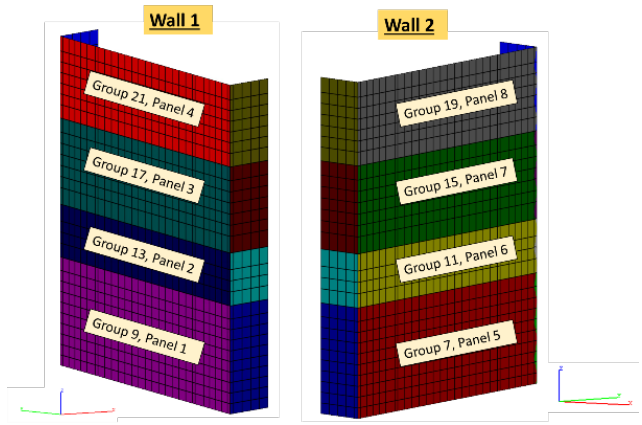

(A) WALL 1 AND 2

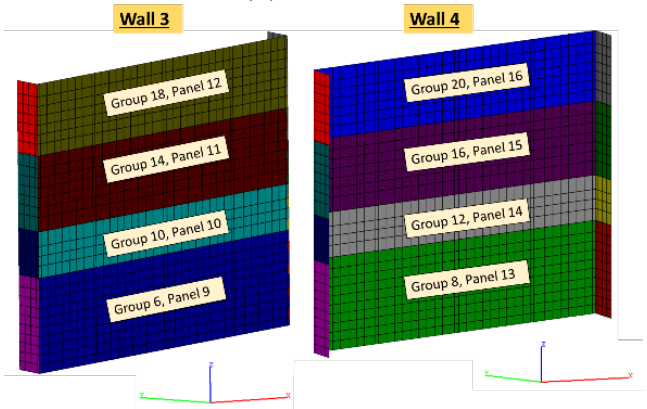

(B) WALL 3 AND 4

FIGURE 5: EXTERIOR RC WALL SUB-MODELS

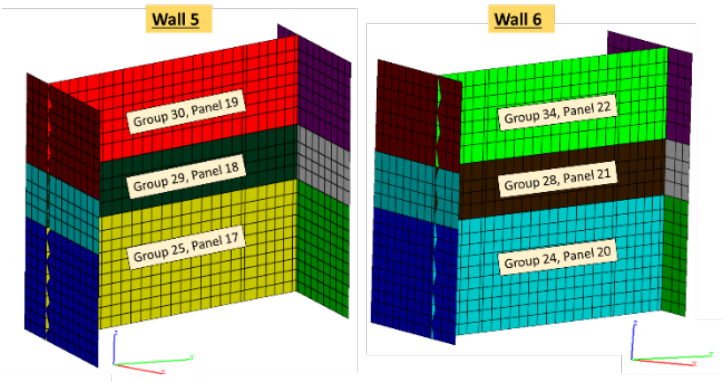

(A) WALL 5 AND 6

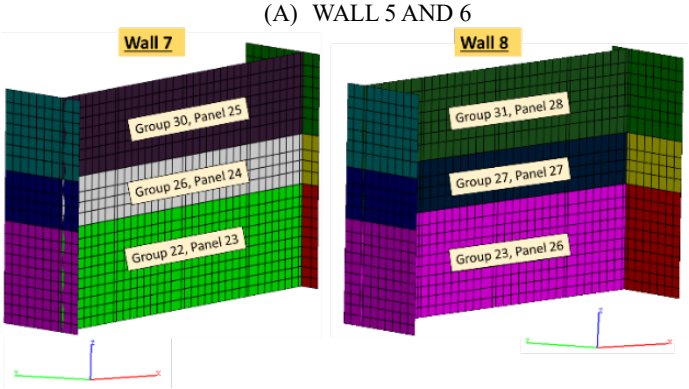

(B) WALL 7 AND 8

FIGURE 6: INTERIOR RC WALL SUB-MODELS

The RC wall panel nonlinear modelling includes two major constitutive components:

1) Back-bone curves (BBCs) for shear and bending deformation for each RC wall at each floor level.
2) Hysteretic models (HMs) for the shear and bending deformation effects for each RC wall panel.

In this study, the following two options are selected.

Option A: *JEAC4601 and AIJ RC Standard Basis*

For shear deformation, Maximum Point-Oriented (PO) shear model in JEAC4601-2015 is selected [5]. For bending deformation, Maximum Point-Oriented Degrade-Trilinear bending model is selected as nonlinear hysteretic models. Each model is shown in Figure 7.

Point 1 for cracking in shear BBC is defined as below.

$$\tau_1 = \sqrt{0.31\sqrt{F_C}\left(0.31\sqrt{F_C} + \sigma_v\right)} \qquad (2)$$
$$\gamma_1 = \tau_1 / G$$

Point 2 for yielding in shear BBC is defined as below.

$$\tau_2 = 1.35\tau_1 \qquad (3)$$
$$\gamma_2 = 3\gamma_1$$

Point 3 for ultimate in shear BBC is defined as below.

$$\tau_3 = \begin{cases} \left(1 - \dfrac{\tau_s}{1.4\sqrt{F_C}}\right)\tau_0 + \tau_s & \text{when } \tau_s \le 1.4\sqrt{F_c} \\ 1.4\sqrt{F_C} & \text{when } \tau_s \ge 1.4\sqrt{F_c} \end{cases} \quad (4)$$

$$\gamma_3 = 0.004$$

where

$$\tau_0 = \left(0.94 - \frac{0.56M}{QD}\right)\sqrt{F_c} \quad (5)$$

$$\text{if } M/QD > 1, \text{ then } M/QD = 1 \quad (6)$$

and where

$$\tau_s = \frac{(P_V + P_H)\cdot \sigma_{sy}}{2} + \frac{(\sigma_V + \sigma_H)}{2} \quad (7)$$

Point 1 for cracking in bending BBC is defined as below.

$$M_1 = Z_e(f_t + \sigma_v)$$
$$\phi_1 = \frac{M_1}{E_C I_e} \quad (8)$$

Point 2 for yielding in bending BBC is defined as below.

$$M_2 = M_y$$
$$\phi_2 = \phi_y \quad (9)$$

Point 3 for ultimate in bending BBC is defined as below.

$$M_3 = M_u$$
$$\phi_3 = \text{Max}\left(\frac{0.004}{X_{nu}}, 20\phi_2\right) \quad (10)$$

The effective flange widths for each RC wall panel are calculated based on AIJ Standard for Structural Calculation of RC Structures [6]. These values are used for calculating section modulus, Z_e for each RC panel.

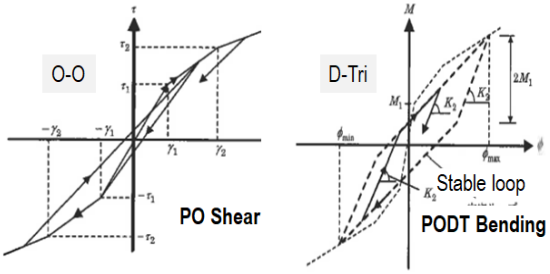

FIGURE 7: Maximum Point-Oriented Hysteretic Models

Option B: *ACI318/ASCE4 and Cheng-Mertz Model Basis*

ACI318 Standard and ASCE4 Standard are applied to the BBC [7,8]. Cheng-Mertz (CM) shear and bending models are applied to shear and bending nonlinear hysteretic models, respectively [9]. Each model is shown in Figure 8.

Point 1 for cracking in shear BBC is defined as below.

$$\tau_1 = 3\sqrt{f_c'}$$
$$\gamma_1 = \tau_1/G \quad (11)$$

Point 2 for yielding in shear BBC is defined as below.

$$\tau_2 = s_r\,\tau_1$$
$$\gamma_2 = \gamma_1\left(1 + 2\left(\frac{\tau_2}{\tau_1} - 1\right)\right) \quad (12)$$

Point 3 for ultimate in shear BBC is defined as below.

$$\tau_3 = \left(\propto \sqrt{f_c'} + P_H f_y\right) \le 8\sqrt{f_c'}$$
$$\gamma_3 = 0.008 \quad (13)$$

Point 1 for cracking in bending BBC is defined as below.

$$M_1 = 7.5\,Z_e\sqrt{f_c'}$$
$$\phi_1 = \frac{M_1}{E_C I_e} \quad (14)$$

Point 2 for yielding in bending BBC is defined as below.

$$M_2 = M_y$$
$$\phi_2 = \phi_y \quad (15)$$

Point 3 for ultimate in bending BBC is defined as below.

$$M_3 = M_u$$
$$\phi_3 = \phi_u \quad (16)$$

The effective flange widths for each RC wall panel are calculated based on ACI318 Standard for Structural Calculation of RC Structures [7].

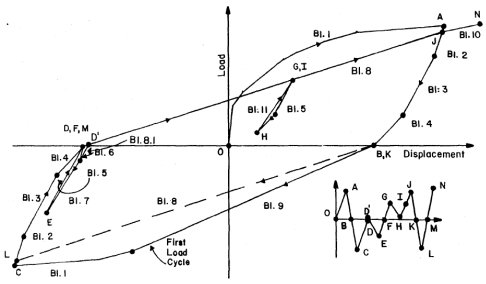

(a) Shear Hysteretic Model

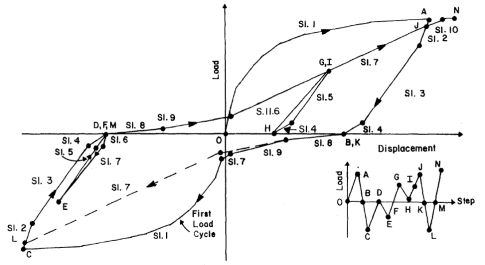

(b) Bending Hysteretic Model

FIGURE 8: CHENG-MERTZ HYSTERETIC MODELS

The material properties used in the analysis model are shown in Table 1.

TABLE 1: MATERIAL PROPERTY

Object	Parameter	Value
Structure	Young's Modulus of Concrete (GPa)	25.7
	Young's Modulus of Steel (GPa)	205
	Poisson Ratio of Concrete (-)	0.2
	Poisson Ratio of Steel (-)	0.3
	Density of RC (kg/m^3)	2300
	Damping Ratio of RC (%)	5
Fluid	Bulk Modulus (GPa)	2.2
	Viscosity (Pa · s)	1.003×10^{-3}
	Density (kg/m^3)	1000

3. RESULTS AND DISCUSSION

The computed BBCs for selected RC walls were compared between Option A (JEAC4601) and Option B (ACI318/ASCE4). For Interior RC Wall (Wall 5), shear and bending BBCs for with-fluid/without-fluid cases are shown in Figure 9 to 12, respectively. There are some differences in BBCs between JEAC4601 and ACI318/ASCE4. Entirely, JEAC4601 BBCs have larger capacities of shear and bending stresses than ACI318/ASCE4 BBCs. Also, JEAC4601 BBCs have smaller shear strains at the ultimate points, because of considering shear span ratio at the ultimate points. In comparison of with-fluid and without-fluid cases for JEAC4601 BBCs, the result confirms that with-fluid case has larger shear and bending capacities at cracking and yielding points comparing with without-fluid case. This is because the formulae of cracking and yielding points in the BBCs include axial stress terms as shown in Eq.(2) and (8).

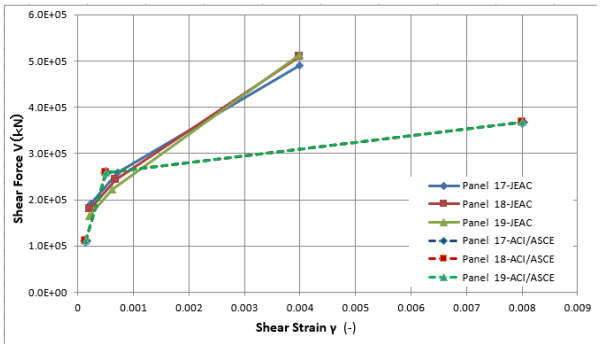

FIGURE 9: SHEAR BBC OF INTERIOR RC WALL (WALL 5) FOR WITHOUT-FLUID CASE

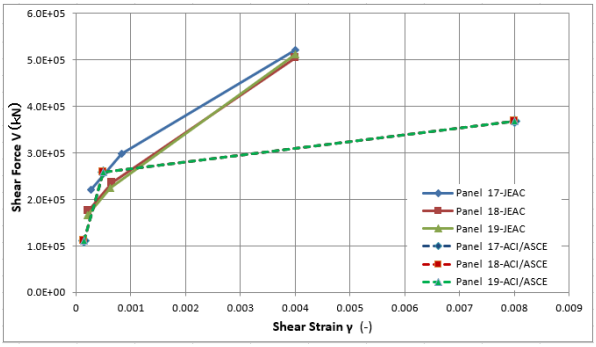

FIGURE 10: SHEAR BBC OF INTERIOR RC WALL (WALL 5) FOR WITH-FLUID CASE

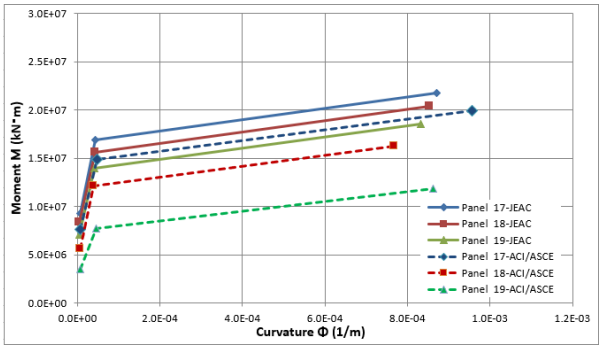

FIGURE 11: BENDING BBC OF INTERIOR RC WALL (WALL 5) FOR WITHOUT-FLUID CASE

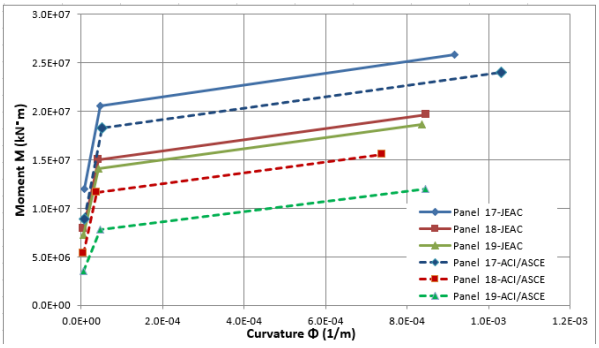

FIGURE 12: BENDING BBC OF INTERIOR RC WALL (WALL 5) FOR WITH-FLUID CASE

Equivalent elastic moduli of shear and bending BBCs for with-fluid cases are shown in Figure 13 and 14. The equivalent elastic moduli were calculated for each nonlinear analysis iteration conducted in ACS SASSI Option NON. It was confirmed that the elastic moduli can be sufficiently converged after two or three iterations. There is not so significant difference of modulus tendency between JEAC4601 and ACI318/ASCE4.

Damping ratios of shear and bending BBCs for with-fluid cases are shown in Figure 15 and 16. It should be noted that damping ratios in ACI318/ASCE4 adopt cut-off criteria of 10% damping in compliance with the maximum damping ratio defined in ASCE4. For shear BBCs, it was confirmed that damping ratios of JEAC4601 can be larger than those of ACI318/ASCE4 due to the damping cut-off in ASCE4. For bending BBCs, it was confirmed that damping ratios in ACI318/ASCE4 were comparable to those in JEAC4601.

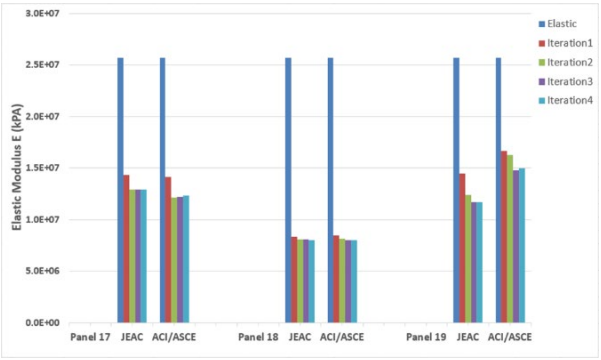

FIGURE 13: EQUIVALENT ELASTIC MODULUS (SHEAR BBC) OF INTERIOR RC WALL (WALL 5) FOR WITH-FLUID CASE

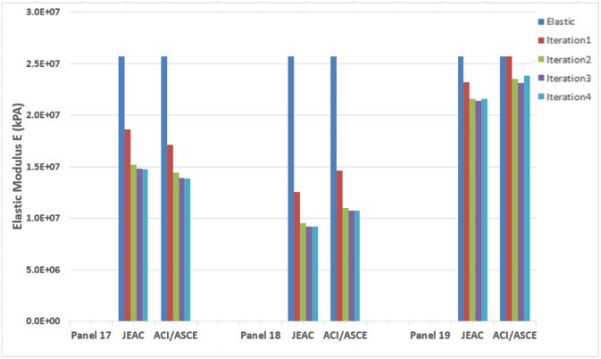

FIGURE 14: EQUIVALENT ELASTIC MODULUS (BENDING BBC) OF INTERIOR RC WALL (WALL 5) FOR WITH-FLUID CASE

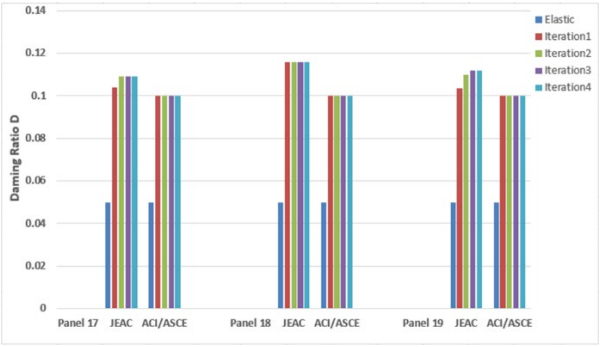

FIGURE 15: DAMPING RATIO (SHEAR BBC) OF INTERIOR RC WALL (WALL 5) FOR WITH-FLUID CASE

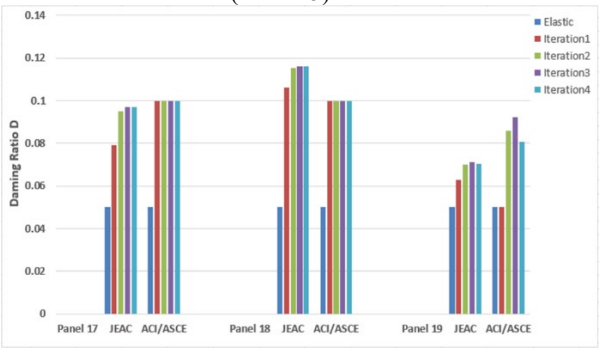

FIGURE 16: DAMPING RATIO (BENDING BBC) OF INTERIOR RC WALL (WALL 5) FOR WITH-FLUID CASE

To confirm the responses of the buildings, acceleration in-structure response spectra (ISRS) were extracted at Node 9206 and 5053 in BLDG15 with-fluid model, as shown in Figure 17. The ISRS for each direction at each node are shown in Figure 18 through 23.

As to Node 9206, for horizontal directions, it was confirmed that the peaks of responses were shifted to the lower frequency side when applying nonlinear analyses. However, there was no obvious difference of seismic responses between JEAC4601 and ACI318/ASCE4. For vertical direction, there was no significant difference between JEAC4601 and ACI318/ASCE4.

As to Node 5053, for horizontal directions, the peaks of responses were shifted to the lower frequency side when applying nonlinear analysis. Also, for X direction, it was confirmed that seismic response of JEAC4601 was lower than that of ACI318/ASCE4 in the frequency range of 6-7 Hz.

As to both Node 9206 and 5053, for horizontal directions, the peak seismic responses of nonlinear analyses tend to be larger than those of elastic responses. The spectral shape of in-column FIRS input motion can be considered to affect the augment of peak seismic responses in nonlinear analyses. The input motion has a peak at around 3 Hz. The shifting of natural frequencies in the building structure can augment the peak responses at around 3 Hz.

The shear and bending hysteretic responses of interior wall panel 18 and 19 are shown in Figure 24 through 27. As an overall behavior, it was confirmed that JEAC4601 maximum PO method provides higher stiffness than Cheng-Mertz method. The results also confirm that Panel 19 has lower responses and provides higher equivalent stiffness than Panel 18.

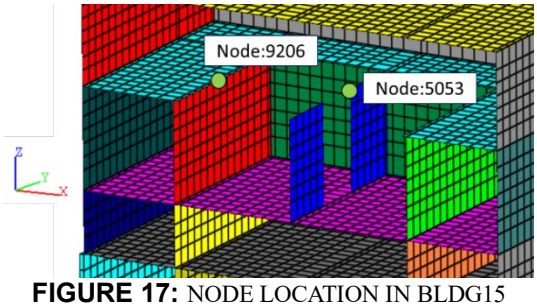

FIGURE 17: NODE LOCATION IN BLDG15 (WITH-FLUID MODEL)

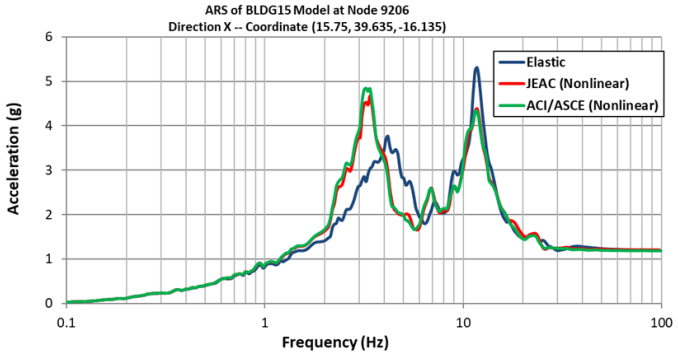

FIGURE 18: ISRS AT NODE 9206 X DIRECTION (WITH-FLUID)

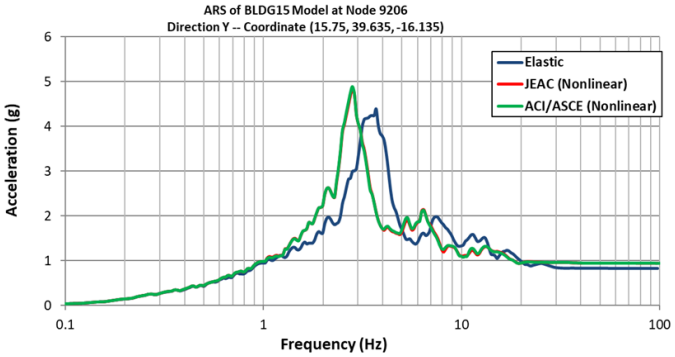

FIGURE 19: ISRS AT NODE 9206 Y DIRECTION (WITH-FLUID)

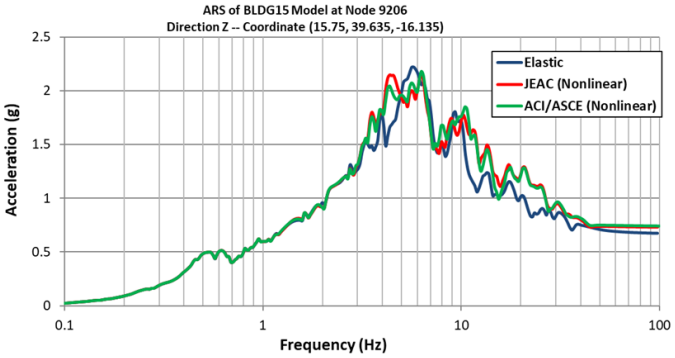

FIGURE 20: ISRS AT NODE 9206 Z DIRECTION (WITH-FLUID)

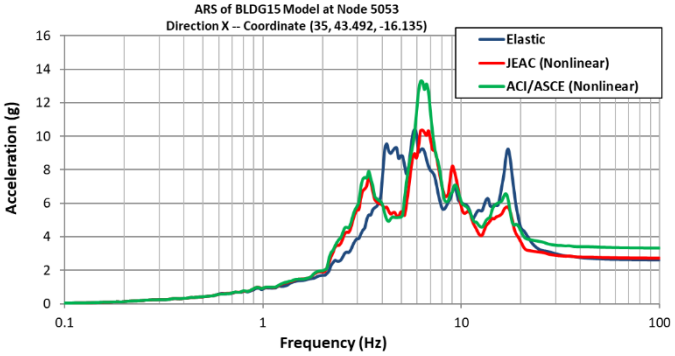

FIGURE 21: ISRS AT NODE 5053 X DIRECTION (WITH-FLUID)

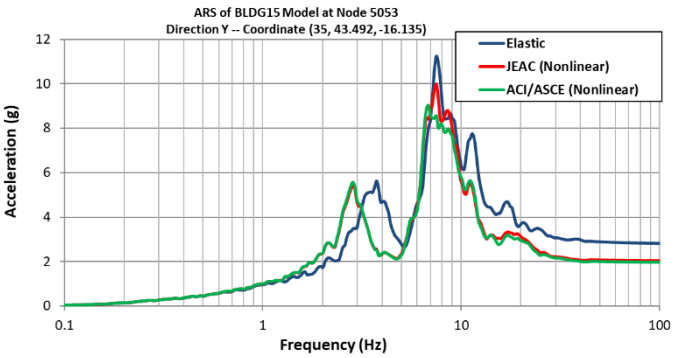

FIGURE 22: ISRS AT NODE 5053 Y DIRECTION (WITH-FLUID)

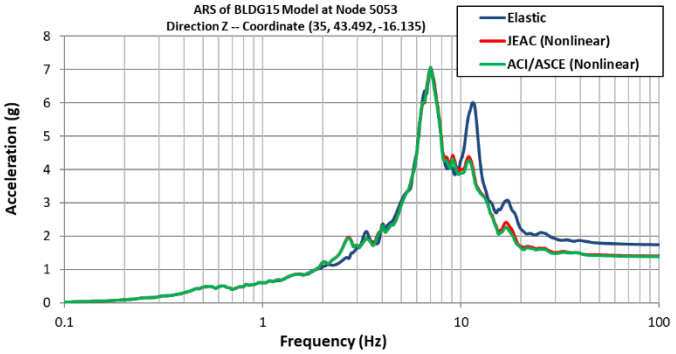

FIGURE 23: ISRS AT NODE 5053 Z DIRECTION (WITH-FLUID)

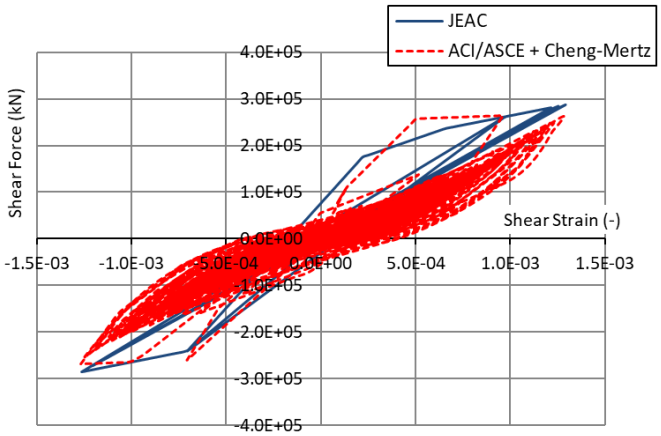

FIGURE 24: SHEAR HYSTERESIS RESPONSES OF INTERIOR WALL PANEL 18 (X-DIRECTION)

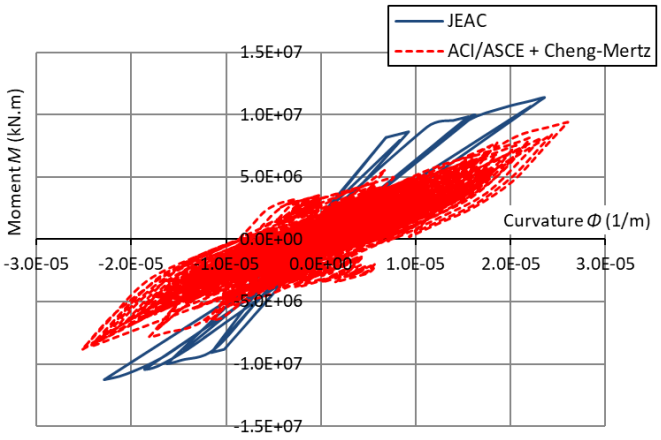

FIGURE 25: BENDING HYSTERESIS RESPONSES OF INTERIOR WALL PANEL 18 (X-DIRECTION)

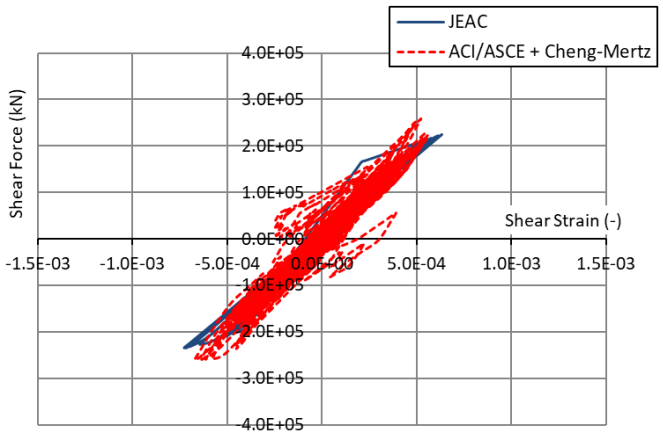

FIGURE 26: SHEAR HYSTERESIS RESPONSES OF INTERIOR WALL PANEL 19 (X-DIRECTION)

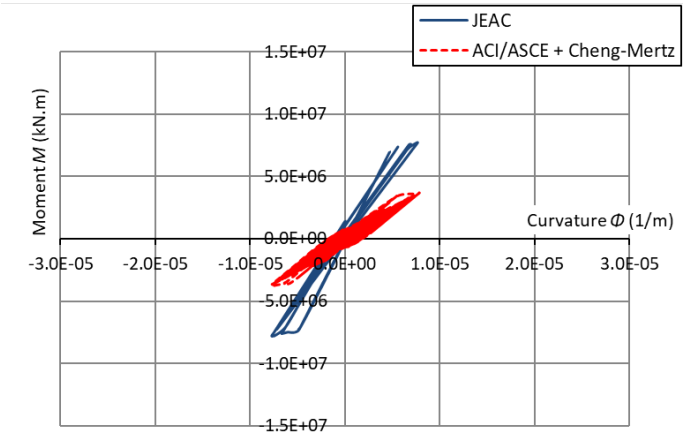

FIGURE 27: BENDING HYSTERESIS RESPONSES OF INTERIOR WALL PANEL 19 (X-DIRECTION)

To confirm the stress distribution on the interior walls, shear stress and bending moments were extracted for Panel 18 and 19. The positions of stress distribution for Panel 18 and 19 are shown in Figure 28 and 32, respectively. The results of stress distributions for panel 18 and 19 are shown in Figure 29 to 31, and Figure 33 to 35, respectively. For panel 18, it was confirmed that the shear and bending stresses of JEAC4601 were comparable to those of ACI318/ASCE4. However, for panel 19, it was confirmed that the shear and bending stresses of JEAC4601 tend to be larger than those of ACI318/ASCE4.

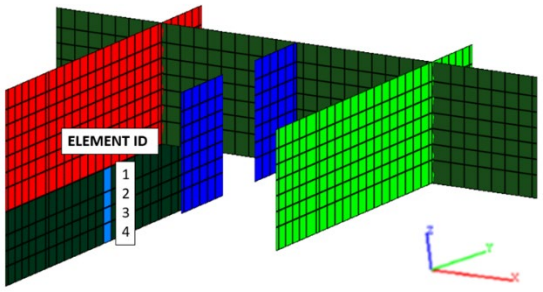

FIGURE 28: POSITION OF STRESS DISTRIBUTION AT PANEL 18

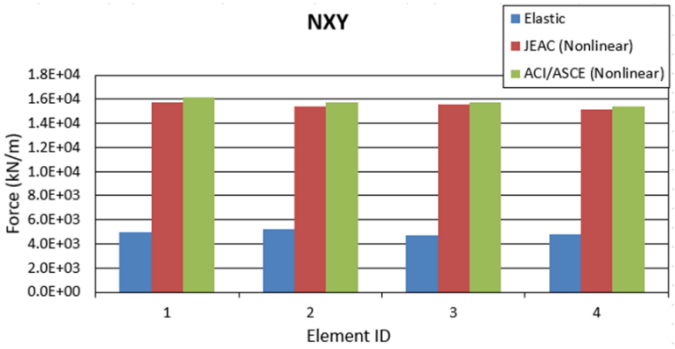

FIGURE 29: MAXIMUM IN-PLANE SHEAR STRESS NXY OF INTERIOR WALL PANEL 18

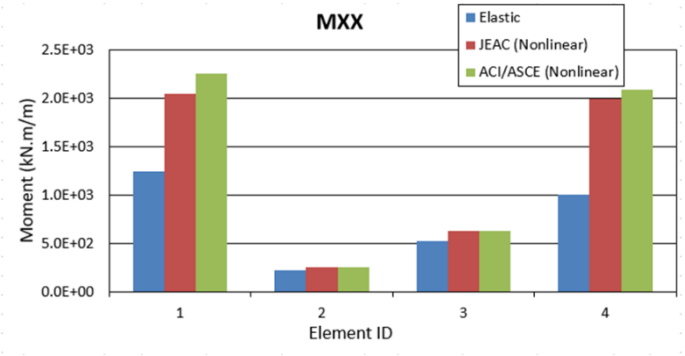

FIGURE 30: MAXIMUM BENDING MOMENT MXX OF INTERIOR WALL PANEL 18

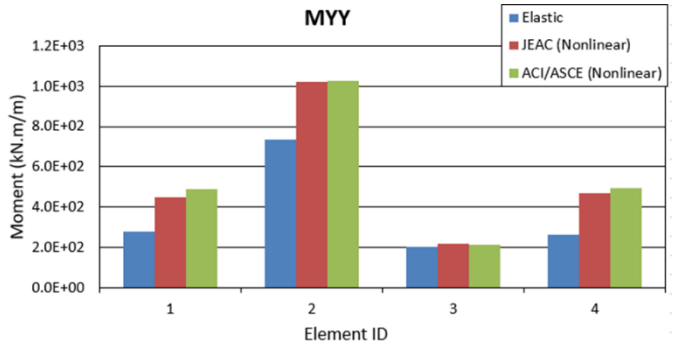

FIGURE 31: MAXIMUM BENDING MOMENT MYY OF INTERIOR WALL PANEL 18

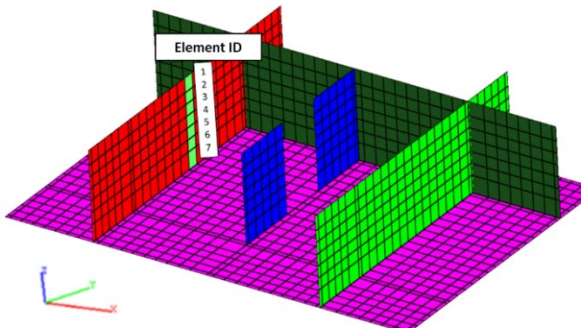

FIGURE 32: POSITION OF STRESS DISTRIBUTION AT PANEL 19

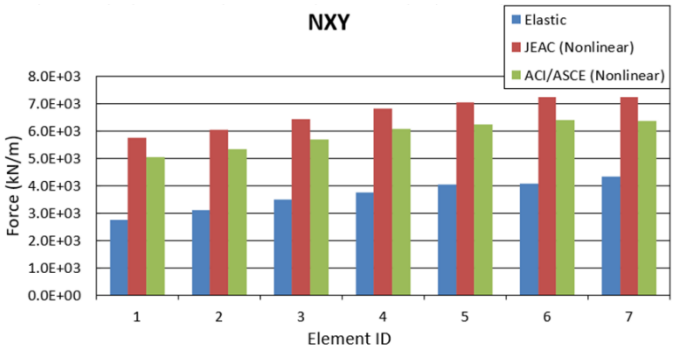

FIGURE 33: MAXIMUM SHEAR STRESS NXY OF INTERIOR WALL PANEL 19

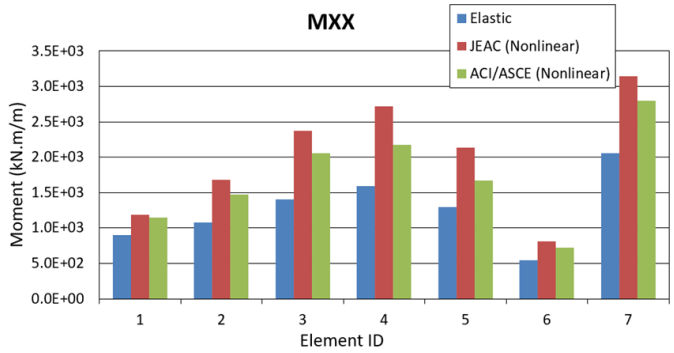

FIGURE 34: MAXIMUM BENDING MOMENT MXX OF INTERIOR WALL PANEL 19

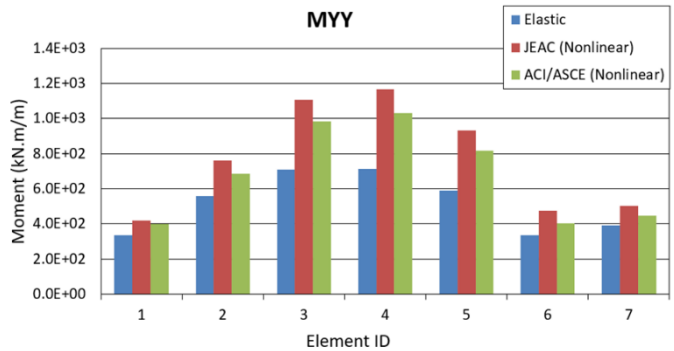

FIGURE 35: MAXIMUM BENDING MOMENT MYY OF INTERIOR WALL PANEL 19

4. CONCLUSION

In this paper, nonlinear characteristics of JEAC4601 and ACI318/ASCE4 were confirmed by applying each code to the state-of-the-art 3D FEM SSI analysis method. By the analysis results, it was confirmed that the differences of formulae in each code were reflected on their seismic responses. As well, the existence of massive water mass in the building can enlarge the difference of seismic responses between each code. The analysis results revealed that the application of JEAC4601 formulae with FSSI analyses is one of solutions for taking into account the fluid mass effect on the nonlinear behavior of RC structures.

REFERENCES

[1] NuScale Power LLC., NuScale Standard Plant Design Certification Application, Revision 5, July 2020.

[2] D.M. Ghiocel, Y. Nitta, R. Ikeda, and T. Shono, Seismic Nonlinear SSI Approach Based on Best Practices in US and Japan. Parts 1: Modeling, SMiRT26, Special Session on Nonlinear Seismic SSI Analysis Based on Best Practices in US and Japan, Berlin, July 10-15, 2022.

[3] Y. Sato, D.M. Ghiocel, S. Kataoka, S. Sato, and Y. Morimoto, Study on Fluid-Structure-Soil-Interaction (FSSI) Effects for A Deeply Embedded Nuclear Facility with A Large-Size Pool Under Severe Earthquakes. Part 1: Linear SSI. SMiRT27 Conference, Division 3, Yokohama, Japan, March 3-8, 2024.

[4] Y. Sato, D.M. Ghiocel, S. Kataoka, and Y. Morimoto, Study on Fluid-Structure-Soil-Interaction (FSSI) Effects for A Deeply Embedded Nuclear Facility with A Large-Size Pool Under Severe Earthquakes. Part 2: Nonlinear SSI. SMiRT27 Conference, Division 3, Yokohama, Japan, March 3-8, 2024.

[5] Nuclear Standard Committee of Japan Electric Association, Technical Code for Aseismic Design of Nuclear Power Plants, Japan Electric Association Code (JEAC 4601-2015), 2016.

[6] Architectural Institute of Japan, AIJ Standard for Structural Calculation of Reinforced Concrete Structures, 2018.

[7] American Concrete Institute, Building Code Requirements for Structural Concrete and Commentary (ACI 318-19), 2020.

[8] American Society of Civil Engineers, Seismic Analysis for Safety-Related Nuclear Structures and Commentary (ASCE 4-16), 2017.

[9] Y.F. Cheng, and G. Mertz, Inelastic Seismic Response of Reinforced Concrete Low-Rise Shear Walls of Building Structures", University of Missouri-Rolla, Dept. of Civil Engineering, CE 89-30, 1989.